catalysts

MDPI

Communication

Boosting Higher Selectivity for Thymol Hydrogenation Reaction over Ni/Ce Catalyst

Haifang Mao [1,2], Yongqi Wu [1], Bo Cui [1], Yun Zhao [1,2] and Xiang Zheng [2,3,*]

[1] School of Chemical and Environmental Engineering, Shanghai Institute of Technology, Shanghai 201418, China; mhf@sit.edu.cn (H.M.); jeremy7777777@foxmail.com (Y.W.); 226062101@sit.edu.cn (B.C.); zhaoyun@sit.edu.cn (Y.Z.)
[2] Shanghai Research Institute of Fragrance and Flavor Industry, Shanghai 200232, China
[3] School of Perfume and Aroma Technology, Shanghai Institute of Technology, Shanghai 201418, China
* Correspondence: zhengxiang@sit.edu.cn

Abstract: The production of menthol via thymol hydrogenation is an industrial technology but is challenging due to the unsatisfied selectivity to menthol. Herein, Ni/Ce catalysts were prepared and used in thymol hydrogenation. A high selectivity of menthol was achieved over Ni_4/Ce_1 catalysts under the optimized reaction condition. Ce incorporation can improve both the activity of Ni catalyst and the selectivity to menthol. To reveal the functions of Ce, catalyst characterizations were conducted. The catalytic activity improvement may be related to the remarkable increase in the surface area of the catalyst and the lower crystalline sizes of Ni that take place when a tiny amount of Ce is incorporated into Ni. Higher selectivity to menthol may be related to the modification of the acidity of an Ni catalyst. In addition, the stability of the Ni_4/Ce_1 catalysts was also evaluated, and after five recycles, the Ni_4/Ce_1 catalysts exhibited outstanding catalytic activity and stability.

Keywords: Ni/Ce catalyst; thymol hydrogenation; menthol

check for updates

Citation: Mao, H.; Wu, Y.; Cui, B.; Zhao, Y.; Zheng, X. Boosting Higher Selectivity for Thymol Hydrogenation Reaction over Ni/Ce Catalyst. *Catalysts* **2023**, *13*, 808. https://doi.org/10.3390/catal13050808

Academic Editors: Dominique Agustin and Jana Pisk

Received: 8 April 2023
Revised: 25 April 2023
Accepted: 26 April 2023
Published: 27 April 2023

Copyright: © 2023 by the authors. Licensee MDPI, Basel, Switzerland. This article is an open access article distributed under the terms and conditions of the Creative Commons Attribution (CC BY) license (https://creativecommons.org/licenses/by/4.0/).

1. Introduction

Menthol, one of the most important fragrances, is widely used in the cosmetic and pharmaceutical industries. The international demand is 34,000 metric tons per year [1]. For menthol synthesis, the starting materials should be highly available. One of the most successful synthetic routes to produce menthol is starting from citral [2]. However, the drawback of this synthetic route is the use of chiral and homogeneous catalysts, leading to recycling difficulties. Another important synthetic route to produce menthol was developed by Symrise, starting with the alkylation of m-cresol with propene to form thymol, then transformed to menthol via hydrogenation [3–5]. The advantage of this process is the use of a heterogeneous catalyst, which can be easily separated from the reaction system or be used in a fixed bed reactor. Thymol hydrogenation is one of the most important reactions in the synthetic route to produce menthol. Many kinds of heterogeneous catalysts have been reported for thymol hydrogenation. Noble metal catalysts have shown an encouraging performance for the thymol hydrogenation reaction, but the cost of precious metal catalysts is very high. Based on the kinetics study of thymol hydrogenation over a supported Pt catalyst in a 0.3 L autoclave with a magnetic stirrer, the main side product, menthane, generated via a hydrogenolysis reaction, is unavoidable, even at 100 °C [6]. In addition to noble metal, base metal, such as Fe, Co, Ni and Cu, have been widely researched due to their low cost [7–10]. Co/Mn mixed oxides have been reported for thymol hydrogenation. High thymol conversion can be obtained at 170–220 °C and 20 MPa via a fixed bed reactor, and d/l-menthol selectivity of 59% can be obtained. However, unfortunately, the side product is more than 4% [11]. The development of cobalt nanoparticles supported on silica as selective catalysts for arene hydrogenations has been reported, where the yield of menthol isomers is 93% [12]. Raney nickel, the most important base metal hydrogenation catalyst, has showed

high activity for the hydrogenation reaction, but the selectivity to target products can be poor, and the storage and transportation of Raney nickel are complex [13,14]. Therefore, supported Ni catalysts have been reported, where 55% of d/l-menthol could be achieved at 190 °C and 1.5 MPa. The kinetics of thymol hydrogenation over Ni/Cr_2O_3 have been investigated in a batch reactor, and unstable menthol isomers were formed at the initial stage; menthol can be obtained only at high thymol conversion rates [10].

Menthol is a commercial product. Conversion and selectivity improvements are very important for reducing the cost of menthol. A high conversion of thymol can easily be obtained using commercial noble metal or base metal hydrogenation catalysts. The major challenge is to improve the selectivity to menthol and keep the side product below 1%.

CeO_2 is often used as a catalyst or support for oxidation reactions, owing to its high thermal stability and excellent redox property [15–17]. However, it is hardly employed for hydrogenation reactions [18,19]. Herein, we report a composite of Ni/Ce as a catalyst for the hydrogenation of thymol to menthol. The activity of the Ni/Ce catalyst was evaluated. The reaction condition was optimized and the stability of the Ni/Ce catalyst was tested. A series of characterizations were conducted to study the reason why the Ce introduced into the Ni can improve the performance of the hydrogenation catalyst.

2. Results and Discussion

2.1. Structure, Composition and Acidity

XRD patterns were collected to investigate the crystal structure of NiO and CeO_2. In the XRD patterns of the pure NiO catalyst, there were characteristic diffraction peaks of NiO (110), (200) and (220) facets at 2θ = 37.2°, 43.2° and 62.8° (JCPDS 78-0643) [20]. No obvious changes in the position of characteristic diffraction peaks can be observed in Ni_x/Ce_x catalysts, suggesting that a partial replacement of Ni^{2+} by Ce^{4+} in the framework of Ni_x/Ce_x did not take place. As depicted in Figure 1, with an increasing amount of CeO_2, the peaks corresponded to NiO becoming weaker, especially for the Ni_1/Ce_1 sample. This was possibly caused by the dispersion improvement in NiO when introducing CeO_2. The weak peak suggests that the crystalline size of NiO was very small. The average crystalline size of each Ni_x/Ce_x catalyst was determined using the Scherrer equation [21] and is listed in Figure 2. It was noted that pure NiO possessed the largest average particle size of 7.6 nm. With an increasing amount of CeO_2, the crystalline size of NiO decreased sharply and had the smallest average crystalline size of 4~5 nm. These low crystalline sizes of NiO occur when a tiny amount of CeO_2 is incorporated into the NiO [22].

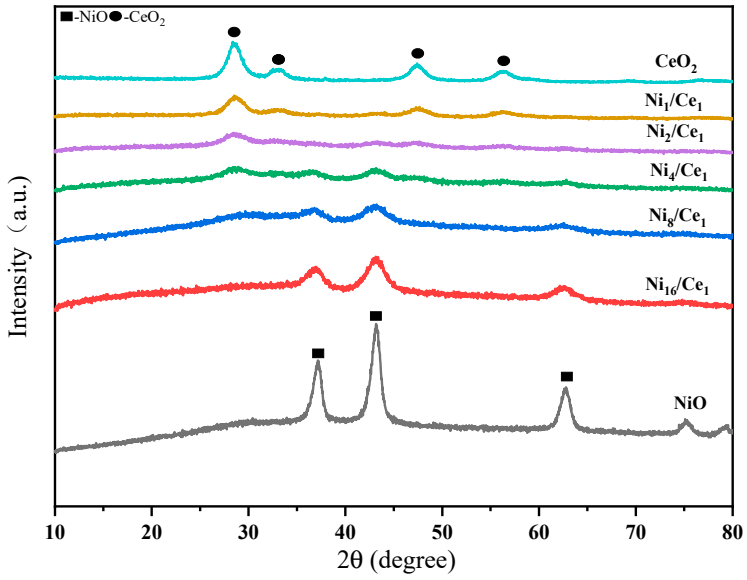


Figure 1. XRD patterns of Ni_x/Ce_x catalysts.

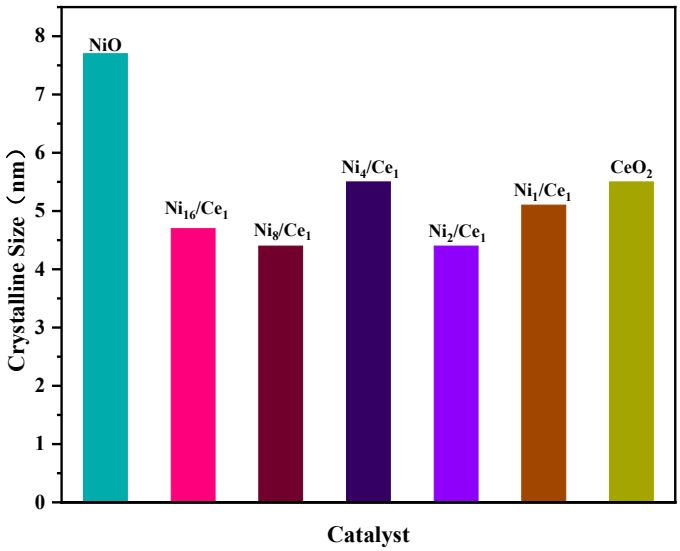


Figure 2. Crystalline size of Ni_x/Ce_x catalysts.

The nitrogen adsorption–desorption isotherms of the Ni_x/Ce_x catalysts at −196 °C are presented in Figure 3. It can be found that each catalyst exhibited a classical Type IV isotherm with a notable hysteresis loop in a relative pressure range of $0.7 < P/P_0 < 1.0$, which indicated the formation of irregular mesoporous characteristics [23]. In addition, the textural properties of the Ni_x/Ce_x catalysts, including the specific surface area (SBET), the average pore diameter and pore volume, are summarized in Table 1. Obviously, the specific surface area of the pure NiO catalyst was relatively low, about 64 m^2/g. With the incorporation of CeO_2, the specific surface area of Ni_{16}/Ce_1 catalysts increased to higher than 100 m^2/g. Ce incorporation can improve the thermal stability of NiO and maintain the higher specific surface area of the Ni_x/Ce_x catalysts after calcination [24]. A higher specific surface area in the catalyst may provide more active sites for thymol hydrogenation, boosting the catalytic activity for thymol hydrogenation.

Table 1. Textural properties of the Ni_x/Ce_x catalysts.

Catalysts	SBET (m^2/g)	Pore Volume (cm^3/g)	Pore Diameter (nm)
NiO	64.1	0.14	7.6
Ni_{16}/Ce_1	104.0	0.26	9.9
Ni_8/Ce_1	97.5	0.24	10.3
Ni_4/Ce_1	91.0	0.37	15.7
Ni_2/Ce_1	93.3	0.25	11.7
Ni_1/Ce_1	55.7	0.25	17.6
CeO_2	50.9	0.18	14.4

Figure 4 shows the Raman spectra of the Ni_x/Ce_x catalysts. For the pure NiO catalyst, there is a weak band at 500 cm^{-1}, which is assigned to the Ni-O stretching mode [25,26]. With the incorporation of Ce, two new bands at 450 cm^{-1} and 570 cm^{-1}, respectively, can be observed for the Ni_x/Ce_x catalysts. The strong band at 450 cm^{-1} is assigned to the Ce-O stretching mode. The new band at 570 cm^{-1} may be caused by the interaction between Ni and Ce [27,28].

Acidity is an important factor for thymol hydrogenation because it is generally believed that acid is beneficial for hydrolysis reactions and will result in a more significant side product [29,30]. Therefore, NH_3-TPD was also carried out to test the acidity of Ni_X/Ce_X catalysts. As shown in Figure 5 and Table 2, there is one main peak at 168 °C for the pure NiO catalyst. Rare earth oxides, such as CeO_2, La_2O_3 and Eu_2O_3, are regarded as basicity oxides, and the acidity of rare earth oxides is weaker than transition metal oxides [31,32].

As expected, with the incorporation of Ce in the Ni_x/Ce_x catalysts, the main desorption peak shifts to lower temperature, which may be caused by the Ni-O-Ce interaction, and led to a decrease in acidic sites and weakened the acidic strength. The acidic sites promote the hydrogenolysis reaction and result in lower selectivity for the hydrogenation reaction [33]. Thus, Ni_x/Ce_x catalysts can show much better selectivity than the Ni catalyst.

Table 2. NH_3-TPD of Ni_x/Ce_x catalysts.

Catalysts	NH_3 Desorption Peak Area
NiO	325
Ni_{16}/Ce_1	268
Ni_8/Ce_1	243
Ni_4/Ce_1	241
Ni_2/Ce_1	143
Ni_1/Ce_1	142
CeO_2	226

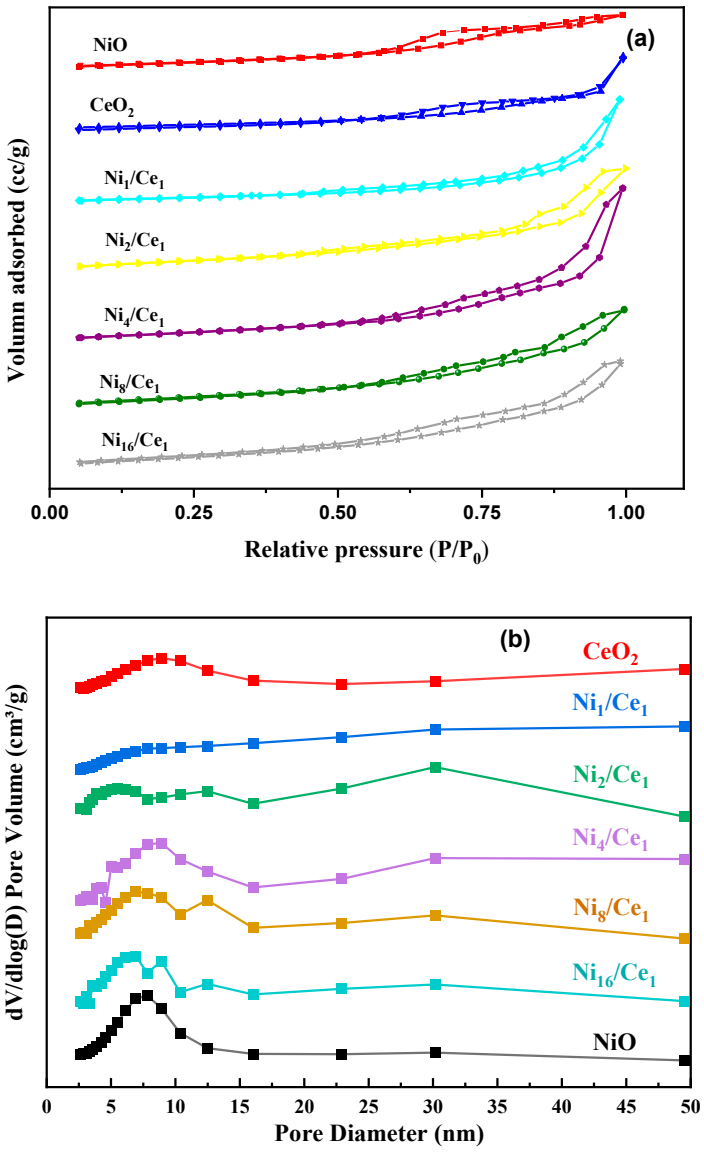


Figure 3. Nitrogen adsorption–desorption isotherms (**a**) of the Ni_x/Ce_x catalysts, pore size distribution curves (**b**) of Ni_x/Ce_x catalyst.

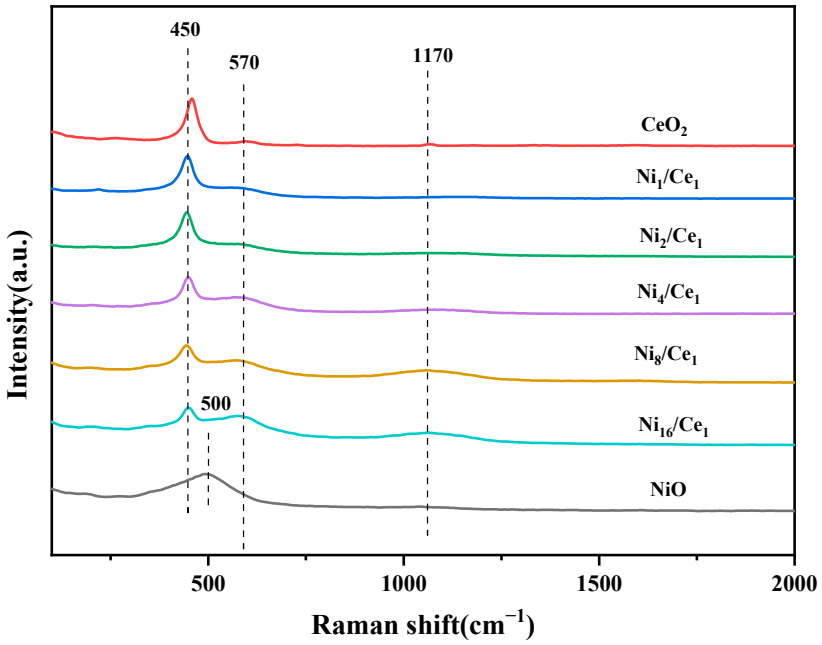


Figure 4. Raman Spectra of Ni_x/Ce_x catalysts.

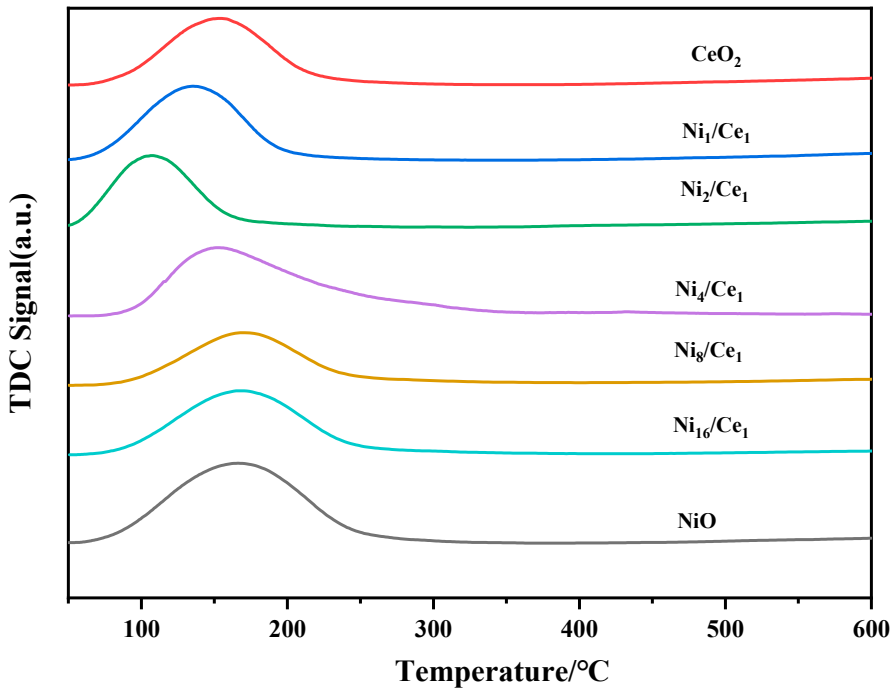


Figure 5. NH_3-TPD profiles of Ni_x/Ce_x catalysts.

H_2-TPD was also carried out to study H_2 adsorption and activization over Ni_x/Ce_x catalysts. As shown in Figure 6 and Table 3, there is a weak H_2 desorption peak at 100–150 °C for the pure NiO catalyst. With the incorporation of Ce in the Ni_x/Ce_x catalysts, one broad and strong H_2 desorption peak can be observed. Ce incorporation can improve the H_2 adsorption. The Ni_4/Ce_1 catalysts possessed a high H_2 adsorption capability, which is favorable for higher catalytic activity for thymol hydrogenation reactions.

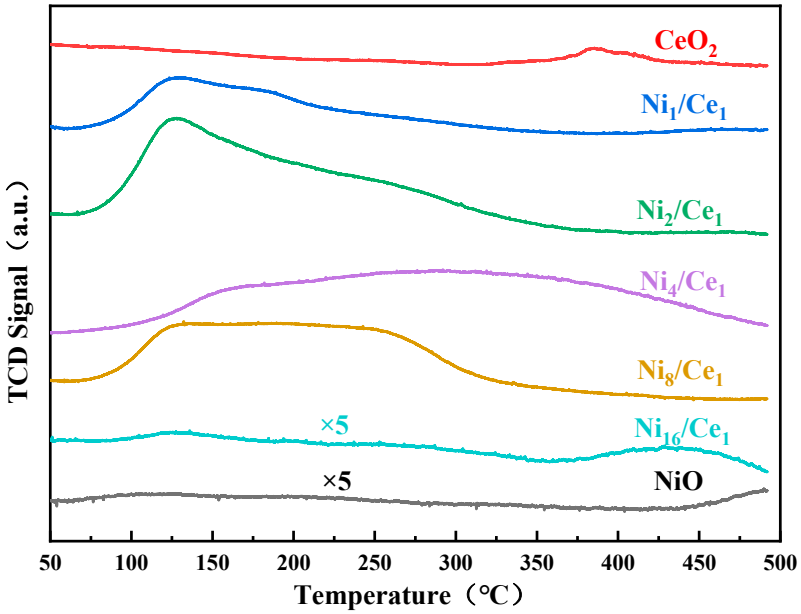


Figure 6. H_2-TPD profiles of Ni_x/Ce_x catalysts.

Table 3. Peak area of H_2 desorption.

Catalysts	Peak Area
NiO	8.8
Ni_{16}/Ce_1	29.4
Ni_8/Ce_1	426.7
Ni_4/Ce_1	607.2
Ni_2/Ce_1	466.8
Ni_1/Ce_1	90.3
CeO_2	71.0

TEM was employed to observe the particle size and the structure of the Ni_4/Ce_1 catalyst. As shown in Figure 7a–c, the average size of the Ni_4/Ce_1 catalyst was about 5 nm. The EDX element mappings (Figure 7d–g) of Ni_4/Ce_1 catalyst indicate that the nanoparticles of the Ni_4/Ce_1 catalyst were composed of both Ni and Ce elements, which were uniformly dispersed, and non-isolated Ni and Ce nanoparticles.

2.2. Evaluation of Catalysts

Thymol hydrogenation reactions were carried out under reaction conditions of 190 °C and 6 Mpa H_2, with a reaction time of 6 h. The performances of Ni_x/Ce_x catalysts are listed in Table 4. The pure Ni catalyst showed some activity for the thymol hydrogenation reaction, but the selectivity of the side product, menthane, was about 9.5%, which is unsatisfied. Ni catalysts show higher activity for hydrogenation reactions, but the selectivity should be improved through catalyst modification [34]. As a result of the incorporation of Ce, higher selectivity of the target products can be achieved over the Ni_4/Ce_1 catalyst, and the selectivity of the side product can be controlled at below 0.4%. With an increase in the molar ration of Ce/Ni, the selectivity of the side product decreased sharply from 9.5% to 0.4%. Based on the NH_3-TPD results, the incorporation of Ce can lead to a decrease in acidic sites' amount and weaken the acidic strength, resulting in higher selectivity for thymol hydrogenation. Fortunately, the conversion of thymol can also be improved over the Ni_x/Ce_x catalyst. With an increase in the molar ration of Ce/Ni, the conversion of thymol increases gradually and then decreases sharply. Based on the XRD and specific surface area results, a higher specific surface area and small crystalline size of Ni can be obtained over the Ni_4/Ce_1 catalyst, which can provide more active sites for thymol

hydrogenation, boosting the catalytic activity for thymol hydrogenation. However, too much Ce incorporation will result in low catalytic activity for thymol hydrogenation. Thus, the molar ratio of Ni/Ce should be controlled to maintain the best performance for the thymol hydrogenation reaction.

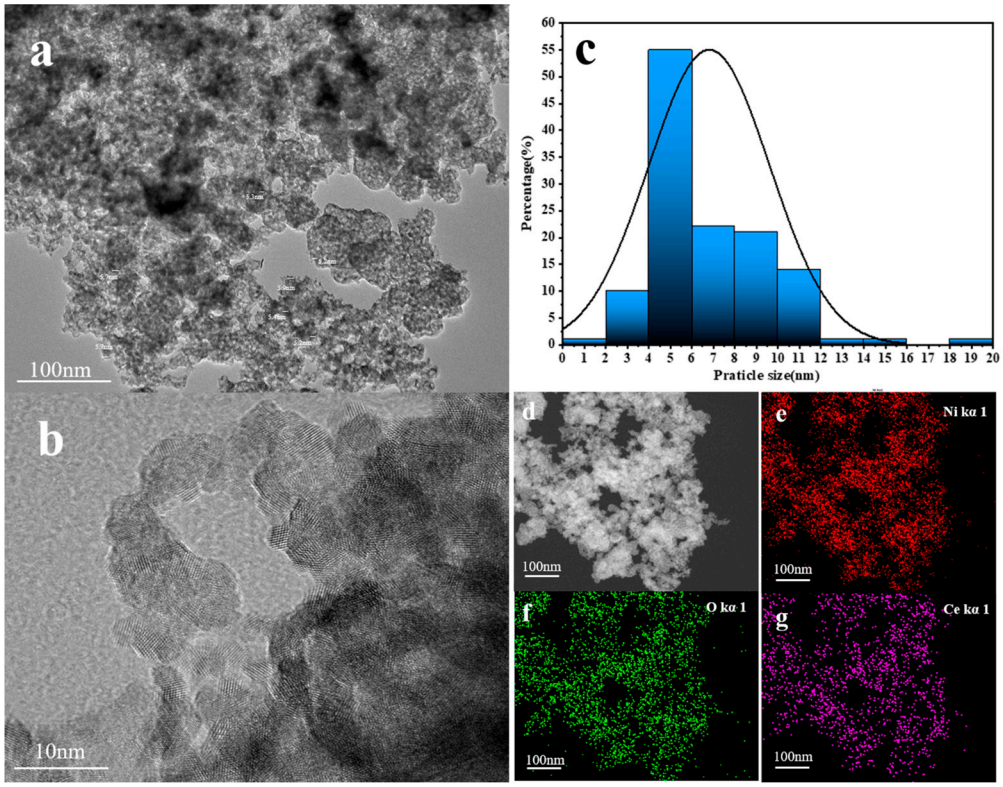


Figure 7. TEM images of (**a**,**b**) Ni_4/Ce_1 catalyst, EDX mapping of (**d**–**g**) Ni_4/Ce_1 catalyst, particle size distribution of (**c**) Ni_4/Ce_1 catalyst.

Table 4. Catalytic performance of different catalysts for thymol hydrogenation reaction.

Entry	Catalysts	Conversion/% Thymol	Selectivity% Menthol + Isomer	Selectivity% Menthol	Selectivity% Side Product
1	NiO	92.3	90.5	47.7	9.5
2	Ni_{16}-Ce_1	>99	96.8	53.4	3.2
3	Ni_8-Ce_1	>99	99.5	55.8	0.5
4	Ni_4-Ce_1	>99	99.6	56.3	0.4
5	Ni_2-Ce_1	>99	99.5	55.8	0.5
6	Ni_1-Ce_1	65.0	99.6	36.2	0.4
7	CeO_2	<1	~	~	~

Reaction conditions: 0.8 g of catalysts, 40 g thymol, 190 °C, 6.0 h; 6 MPa H_2 pressure.

The effects of H_2 pressure and reaction temperature were investigated, and the results are displayed in Tables 5 and 6. The reaction rate of the hydrogenation reaction is fast at higher temperatures and higher H_2 pressures. However, the selectivity of the target product is dissatisfactory under higher reaction temperatures and higher H_2 pressures [35]. As depicted in Table 5, the Ni_4/Ce_1 catalyst showed low activity at a lower reaction temperature, and thymol cannot be totally converted when the reaction temperature is below 190 °C for 6 h. A thymol conversion of 99.0% can only be obtained when the reaction temperature is higher than 190 °C. As the reaction temperature increased from 150 °C to 200 °C, the selectivity of the side product slightly increased. Even when the reaction temperature increased to 200 °C, the selectivity of the side product, menthane,

was only 0.6%, which suggests that Ni_4/Ce_1 catalysts have better selectivity for thymol hydrogenation, even at higher reaction temperatures. From Table 6, it can be seen that high H_2 pressure is beneficial for improving the conversion of thymol. Thymol can be totally converted at an H_2 pressure 6 MPa. The selectivity of menthol was almost unchanged when the H_2 pressure increased from 2 MPa to 6 MPa.

Table 5. Effect of reaction temperature.

Entry	Reaction Temperature (°C)	Conversion/% Thymol	Selectivity% Menthol + Isomer	Selectivity% Menthol	Selectivity% Side Product
1	150	37.6	99.9	30.0	0.1
2	160	41.1	99.8	37.8	0.2
3	170	71.4	99.7	39.4	0.3
4	180	81.3	99.7	41.7	0.3
5	190	>99	99.6	56.3	0.4
6	200	>99	99.4	54.2	0.6

Reaction conditions: 0.8 g of catalysts, 40 g thymol, 6.0 h, 6 MPa H_2 pressure.

Table 6. Effect of H_2 pressure.

Entry	H_2 Pressure (MPa)	Conversion/% Thymol	Selectivity/% Menthol + Isomer	Selectivity/% Menthol	Selectivity/% Side Product
1	2	31.1	99.8	28.6	0.2
2	3	54.8	99.6	34.9	0.4
3	4	64.3	99.8	37.5	0.2
4	5	74.3	99.9	46.2	0.1
5	6	>99	99.6	56.3	0.4

Reaction conditions: 0.8 g of catalysts, 40 g thymol, 6.0 h, 190 °C.

In addition to the selectivity to the target product and activity of the catalysts, the stability of heterogeneous catalysts is another significant characteristic for heterogeneous catalysts [36,37]. However, the conversion of thymol is close to 100% at 190 °C regarding the Ni_4/Ce_1 catalyst, which would be confusing in the assessment of catalyst stability. In general, the stability test should be carried out at lower conversion rates. Therefore, we conducted the catalyst stability test at a reaction temperature of 190 °C and reaction time of 4 h. The conversion of thymol can be controlled at below 90%. It can be seen from Table 7 that, after five recycle runs, the catalyst could still perform well, with only a slight decrease in the conversion of thymol, indicating that the Ni_4/Ce_1 catalyst had good stability.

Table 7. The recycle stability of Ni_4/Ce_1 catalyst.

Entry	Recycle Number	Conversion/% Thymol	Selectivity/% Menthol + Isomer	Selectivity/% Side Product
1		89	99.6	0.4
2	1	88	99.7	0.3
3	2	89	99.6	0.4
4	3	89	99.7	0.3
5	4	87	99.6	0.4
6	5	88	99.6	0.4

Reaction conditions: 0.8 g of catalysts, 40 g thymol, 4.0 h, 6 MPa H_2 pressure, 190 °C.

3. Experimental

3.1. Materials

The chemical reagents used included nickel acetate, cerium acetate and Na_2CO_3. All the above reagents of analytical grade were purchased from Adamas and used as received without pretreatment.

3.2. Preparation of NiO/CeO_2 Catalyst

NiO/CeO_2 was prepared via coprecipitation method. As is typical, nickel acetate and cerium acetate were dissolved in 100 mL deionized water under stirring at room temperature; then, they were slowly added into the solution of Na_2CO_3 under stirring at room temperature for 1 h. After aging at room temperature for 2 h, the precipitate was separated by filtering and washed with deionized water three times. After drying the filter cake at 110 °C for 12 h and then calcining at 400 °C for 4 h, the back NiO/CeO_2 composite powder was obtained. Different molar ratios of NiO/CeO_2 can be obtained via the above method. The method was utilized, changing the molar ratio of NiO/CeO_2 with 16:1, 8:1, 4:1, 2:1 and 1:1, denoted as Ni_{16}/Ce_1, Ni_8/Ce_1, Ni_4/Ce_1, Ni_2/Ce_1 and Ni_1/Ce_1, respectively.

3.3. Catalyst Evaluation

The hydrogenation of thymol was performed in a stainless-steel autoclave. The catalysts were pretreated by H_2 at 350 °C for 4 h before being used in hydrogenation reaction. Typically, 0.8 g of catalysts and 40 g thymol were added into the autoclave reactor. The autoclave reactor was purged with N_2 3 times and finally charged with H_2 to a certain pressure at room temperature, and then heating was started, the stirring was switched and stirring speed was kept at 500 r/min.

After the reaction, the liquid products were separated by centrifuging and analyzed by gas chromatography of GC9790 series with SE-54 column.

3.4. Catalyst Characterization

XRD patterns were recorded on Bruker D2 PHASER, using Cu Kα radiation and operating at 40 kV and 40 mA. The scanning range was set from 10° to 80° (2θ), with a step size of 5°/min.

The Brunauer–Emmett–Teller (BET) specific surface areas of typical products were obtained using Micrometrics ASAP2020 HD88 multi-function nitrogen adsorption instrument. Firstly, the test sample was degassed in vacuum at 200 °C for 8 h and then determined at −196 °C. The specific surface area data were obtained according to the Brunauer–Emmett–Teller (BET) equation.

Raman experiment was adopted using HORIBA Scientific LabRAM HR Evolution instrument, with an excitation wavelength of 514 nm.

NH_3-TPD experiments were performed in a Micromeritics AutoChem II 2920 with a thermal conductivity detector. A 50 mg sample was pre-treated at 400 °C under He flow and then cooled down to room temperature. It was filled with NH_3 to achieve adsorption saturation, and then the sample was heated from 50 °C to 800 °C.

H_2-TPD experiments were performed in a quartz micro-reactor with a thermal conductivity detector. A 100 mg sample was pre-treated at 350 °C under H_2 flow for 4 h and then cooled down to room temperature under N_2. It was filled with H_2 to achieve adsorption saturation at 50 °C for 1 h, followed by N_2 flushing for another 1 h to remove the physical absorption H_2, and then the sample was heated from 50 °C to 500 °C under N_2. Thermal conductivity detector recorded the signal. Transmission electron microscope (TEM) images were obtained with HRTEM 2010 JEOL (200 kV). The average Ni particle sizes were determined using ImageJ software.

4. Conclusions

In conclusion, Ni_x/Ce_x catalysts were prepared and applied in thymol hydrogenation. Ce incorporation can improve both the activity of Ni catalysts and the selectivity to menthol. Under the optimized conditions, a thymol conversion of 99.0% and menthol + isomer selectivity of 99.6% were harvested over the Ni_4/Ce_1 catalyst. Combining the characterizations of the catalysts, Ce incorporation can improve the thermal stability of Ni and maintain the higher specific surface area of the Ni_x/Ce_x catalysts after calcination. Benefitting from the larger specific surface area and smaller crystalline size of the catalyst, the Ni_4/Ce_1 catalyst presented a superior catalytic performance. Ce incorporation led to a decrease in acidic

sites' amount and weakened the acidic strength, resulting in high menthol selectivity. In addition, the Ni_4/Ce_1 catalyst had high stability and still performed well after five recycle runs. This study supplies a strategy for developing efficient and stable Ni-based catalysts in terms of hydrogenation reaction.

Author Contributions: H.M.; writing—review and editing, Y.W.; writing—original draft preparation, B.C.; investigation, Y.Z.; methodology, X.Z.; writing—review and editing. All authors have read and agreed to the published version of the manuscript.

Funding: This work was supported financially by the Shanghai Engineering Technology Research Center of Shanghai Science and Technology Commission, grant number 20DZ2255600, the Collaborative Innovation Center of Fragrance Flavor and Cosmetics, XTCXC-202101, and the Shanghai Rising-Star Program, 23QB1405000.

Data Availability Statement: Not applicable.

Conflicts of Interest: The authors declare no conflict of interest.

References

1. Dylong, D.; Hausoul, P.J.; Palkovits, R.; Eisenacher, M. Synthesis of menthol: Industrial synthesis routes and recent development. *Flavour Fragr. J.* **2002**, *37*, 195–209. [CrossRef]
2. Noyori, R. Asymmetric catalysis: Science and opportunities (Nobel lecture 2001). *Adv. Synth. Catal.* **2003**, *345*, 15–32. [CrossRef]
3. Gerhard, D.; Gerd, M.P.; Bayer, A.G. Process for Preparing D,L Menthol from D-Menthol. U.S. Patent US5756864, 26 May 1998.
4. Biedermann, W.; Koeller, H.; Wedemeyer, K.; Bayer, A.G. Method of Production Thymol. German Patent DE2528303, 16 February 1978.
5. Wimmer, P.; Buysch, H.J.; Puppe, L.; Bayer, A.G. Production Technology of Thymol. German Patent Application DE3824284, 18 January 1990.
6. Besson, M.; Bullivant, L.; Nicollaus, N.; Gallezot, P. Stereoselective thymol hydrogenation, I: Kinetics of thymol hydrogenation on charcoal-supported platinum catalysts. *J. Catal.* **1993**, *140*, 30–40. [CrossRef]
7. Barney, A.L.; Hass, H.B. Racemic menthol. New synthesis from thymol. *Ind. Eng. Chem.* **1944**, *36*, 85–87. [CrossRef]
8. Brode, W.R.; Van Dolah, R.W. Synthesis of racemic menthol. *Ind. Eng. Chem.* **1947**, *39*, 1157–1160. [CrossRef]
9. Allakhverdiev, A.I.; Kulkova, N.V.; Murzin, D.Y. Liquid-phase stereoselective thymol hydrogenation over supported nickel catalysts. *Catal. Lett.* **1994**, *29*, 57–67. [CrossRef]
10. Allakhverdiev, A.I.; Kulkova, N.V.; Murzin, D.Y. Kinetics of thymol hydrogenation over a Ni-Cr_2O_3 catalyst. *Ind. Eng. Chem. Res.* **1995**, *34*, 1539–1547. [CrossRef]
11. Biedermann, W.; Bayer, A.G. Method of Production D,L-Menthol. German Patent DE2314813, 22 June 1978.
12. Murugesan, K.; Senthamarai, T.; Alshammari, A.S.; Altamimi, R.M.; Kreyenschulte, C.; Pohl, M.M.; Lund, H.; Jagadeesh, R.V.; Beller, M. Cobalt-nanoparticles catalyzed efficient and selective hydrogenation of aromatic hydrocarbons. *ACS Catal.* **2019**, *9*, 8581–8591. [CrossRef]
13. Da Costa, P. Ni-Containing Catalysts. *Catalysts* **2021**, *11*, 645. [CrossRef]
14. Falabella Sousa-Aguiar, E.; Zanon Costa, C.; Peixoto Gimenes Couto, M.A.; De Almeida Azevedo, D.; De Carvalho Filho, J.F.S. Conversion of residual palm oil into green diesel and biokerosene fuels under sub-and supercritical conditions employing aney Nickel as catalyst. *Catalysts* **2021**, *11*, 995. [CrossRef]
15. Montini, T.; Melchionna, M.; Monai, M.; Fornasiero, P. Fundamentals and catalytic applications of CeO_2-based materials. *Chem. Rev.* **2016**, *116*, 5987–6041. [CrossRef] [PubMed]
16. Paier, J.; Penschke, C.; Sauer, J. Oxygen defects and surface chemistry of ceria: Quantum chemical studies compared to experiment. *Chem. Rev.* **2013**, *113*, 3949–3985. [CrossRef] [PubMed]
17. Sato, S.; Sato, F.; Gotoh, H.; Yamada, Y. Selective dehydration of alkanediols into unsaturated alcohols over rare earth oxide catalysts. *ACS Catal.* **2013**, *3*, 721–734. [CrossRef]
18. Yan, X.H.; Sun, J.P.; Li, B.; Lu, X.; Sun, M.F. Liquid-phase hydrogenation of chloronitrobenzene to chloroaniline over Ni-Ce-P amorphous alloy catalyst. *Chin. J. Catal.* **2006**, *272*, 178–182.
19. Greluk, M.; Gac, W.; Rotko, M.; Slowik, G.; Turczyniak-Surdacka, S. Co/CeO_2 and Ni/CeO_2 catalysts for ethanol steam reforming: Effect of the cobalt/nickel dispersion on catalysts properties. *J. Catal.* **2021**, *393*, 159–178. [CrossRef]
20. Abdelbaki, Y.; De Arriba, A.; Issaadi, R.; Sanchez-Tovar, R.; Solsona, B.; Nieto, J.M.L. Optimization of the performance of bulk NiO catalyst in the oxidative dehydrogenation of ethane by tuning the synthesis parameters. *Fuel Process. Technol.* **2022**, *229*, 107182. [CrossRef]
21. Zenou, V.Y.; Bakardjieva, S. Microstructural analysis of undoped and moderately Sc-doped TiO_2 anatase nanoparticles using Scherrer equation and Debye function analysis. *Mater. Charact.* **2018**, *144*, 287–296. [CrossRef]
22. Solsona, B.; Concepcion, P.; Hernandez, S.; Demicol, B.; Nieto, J.M.L. Oxidative dehydrogenation of ethane over NiO-CeO_2 mixed oxides catalysts. *Catal. Today* **2012**, *180*, 51–58. [CrossRef]

23. Wang, N.; Shen, K.; Huang, L.H.; Yu, X.P.; Qian, W.Z.; Chu, W. Facile Route for synthesizing ordered mesoporous Ni-Ce-Al Oxide materials and their catalytic performance for methane dry reforming to hydrogen and syngas. *ACS Catal.* **2013**, *3*, 1638–1651. [CrossRef]
24. Gonzalez-DelaCruz, V.M.; Holgado, J.P.; Pereniguez, R.; Caballero, A. Morphology changes induced by strong metal-support interaction on a Ni-ceria catalytic system. *J. Catal.* **2008**, *257*, 307–314. [CrossRef]
25. Savova, B.; Loridant, S.; Filkova, D.; Millet, J.M.M. Ni-Nb-O catalysts for ethane oxidative dehydrogenation. *Appl. Catal.* **2010**, *390*, 148–157. [CrossRef]
26. Heracleous, E.; Lemonidou, A.A. Ni-Nb-O mixed oxides as highly active and selective catalysts for ethene production via ethane oxidative dehydrogenation. Part I: Characterization and catalytic performance. *J. Catal.* **2006**, *237*, 162–174. [CrossRef]
27. Brussino, P.; Bortolozzi, J.P.; Milt, V.G.; Banus, E.D.; Ulla, M.A. NiCe/γ-Al_2O_3 coated onto cordierite monoliths applied to oxidative dehydrogenation of ethane (ODE). *Catal. Today* **2016**, *273*, 259–265. [CrossRef]
28. Liu, Y.M.; Wang, L.C.; Chen, M.; Xu, J.; Cao, Y.; He, H.Y.; Fan, K.N. Highly selective Ce-Ni-O catalysts for efficient low temperature oxidative dehydrogenation of propane. *Catal. Lett.* **2009**, *130*, 350–354. [CrossRef]
29. Guo, Y.; Jing, Y.; Xia, Q.; Wang, Y. NbO_x-based catalysts for the activation of C-O and C-C bonds in the valorization of waste carbon resources. *Acc. Chem. Res.* **2022**, *55*, 1301–1312. [CrossRef]
30. Xia, Q.N.; Cuan, Q.; Liu, X.H.; Gong, X.Q.; Lu, G.Z.; Wang, Y.Q. Pd/$NbOPO_4$ multifunctional catalyst for the direct production of liquid alkanes from aldol adducts of furans. *Angew. Chem.* **2014**, *126*, 9913–9918. [CrossRef]
31. Li, X.; Lu, G.; Guo, Y.; Guo, Y.; Wang, Y.; Zhang, Z.; Liu, X.; Wang, Y. A novel solid superbase of Eu_2O_3/Al_2O_3 and its catalytic performance for the transesterification of soybean oil to biodiesel. *Catal. Commun.* **2007**, *8*, 1969–1972. [CrossRef]
32. Wang, Z.; Fongarland, P.; Lu, G.; Essayem, N. Reconstructed La, Y, Ce-modified MgAl-hydrotalcite as a solid base catalyst for aldol condensation: Investigation of water tolerance. *J. Catal.* **2014**, *318*, 108–118. [CrossRef]
33. Yun, Y.S.; Berdugo-Diaz, C.E.; Flaherty, D.W. Advances in understanding the selective hydrogenolysis of biomass derivatives. *ACS Catal.* **2021**, *11*, 11193–11232. [CrossRef]
34. Sun, Z.; Zhang, Z.H.; Yuan, T.Q.; Ren, X.; Rong, Z. Raney Ni as a versatile catalyst for biomass conversion. *ACS Catal.* **2021**, *11*, 10508–10536. [CrossRef]
35. Vasiliades, M.A.; Govender, N.S.; Govender, A.; Crous, R.; Moodley, D.; Botha, T.; Efstathiou, A.M. The effect of H_2 pressure on the carbon path of methanation reaction on Co/γ-Al_2O_3: Transient isotopic and operando methodology studies. *ACS Catal.* **2022**, *12*, 15110–15129. [CrossRef]
36. Feng, Y.; Liu, Y.X.; Dai, H.X.; Deng, J.G. Review and perspectives of enhancement in the catalytic stability for the complete combustion of CO, CH_4, and volatile organic compounds. *Energy Fuels* **2023**, *37*, 3590–3604. [CrossRef]
37. Lin, H.X.; Liu, Y.X.; Deng, J.G.; Jing, L.; Dai, H.X. Methane combustion over the porous oxides and supported noble metal catalysts. *Catalysts* **2023**, *13*, 427. [CrossRef]

Disclaimer/Publisher's Note: The statements, opinions and data contained in all publications are solely those of the individual author(s) and contributor(s) and not of MDPI and/or the editor(s). MDPI and/or the editor(s) disclaim responsibility for any injury to people or property resulting from any ideas, methods, instructions or products referred to in the content.